AERODYNAMIC DESIGN AND STRESS ANALYSIS OF 100kW RADIAL INFLOW TURBINE FOR ORGANIC RANKINE CYCLE SYSTEM

Lei Chen

Industry Development Division

Heavy Engineering Research Association, New Zealand

lei.chen@hera.org.nz

Keywords: *Aerodynamic design, stress analysis, radial inflow turbine, Organic Rankine Cycle.*

ABSTRACT

The Organic Rankine Cycle (ORC) has been considered to be the most feasible technology among the existing approaches to convert low grade heat source (such as geothermal energy and industrial waste heat) into electricity. Due to the main features of low mass flow rate and high pressure ratio, radial inflow turbines are applied more often than other types of turbines in small scale ORC systems with a general power range of 50kW to 500kW, because they are more efficient, adaptable, stable and cost-effective. When developing such a turbine, the aerodynamic design and the stress analysis are the steps of vital importance. This paper presents the detailed information of the aerodynamic design and the stress analysis of a 100kW radial inflow turbine, including preliminary design, three dimensional modelling of blades and volute, performance evaluation by using Computational Fluid Dynamics (CFD) and stress analysis based on Finite Element Method (FEM). In the step of aerodynamic design, ANSYS turbomachinery module and in-house code are used to design the turbine geometry. The scalloped design of the rotor and the balance piton on the shaft were carried out to reduce the turbine thrust load and match with the requirement of the magnetic bearings. The performance evaluation of the turbine is conducted by using ANSYS CFX, where R245fa was used as the working fluid. Detailed analyses of the flow features across the turbine stage and the volute are presented. In the stress analysis step, the material selection of each component of turbine is completed and the simulation results in terms of equivalent stress and deformation of turbine blades are analysed to confirm the safety of turbine during its operation.

1. INTRODUCTION

New Zealand has extensive geothermal energy resources, which are mainly located at Taupo area (volcanic places) and the full use of them are critical to the economic development, environmental protection and energy security. Meanwhile, nations around the world are making great effort to improve their energy security, preserve the environment and enhance the reduction of the greenhouse gas emissions.

Among the projects proposed to make use of geothermal energy in New Zealand, Above Ground Gerthermal and Allied Technologies (AGGAT) programme is focused on developing Organic Rankine Cycle (ORC) solutions for the waste heat and geothermal markets. It is a perfect example of building a platform to enable others. It brings together the best of academia with practical engineering and the pace of industry drawing on their expertise in research, fabrication, knowledge and experience to deliver new AGGAT products.

The AGGAT diamond, shown in Figure 1, illustrates the contents of research themes of the AGGAT programme.

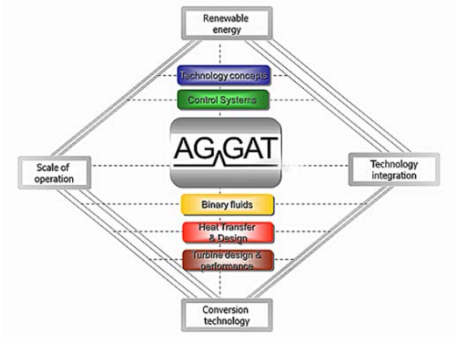

Figure 1: Framework of AGGAT programme

By integrating all the technologies above, the AGGAT programme aims at achieving sustainable economic development through the efficient use of energy resources

The ORC technology is of crucial importance in the power system (Quoilin, 2013). It can have a beneficial effect on the energy intensity of industrial processes, mainly by recovering waste heat; it can have a positive effect on building consumptions, e.g. using Combined Heat Power systems; it can be used to convert renewable heat into electricity. In addition, the Organic Rankine Cycle also shows a number of advantages over the steam cycle (Quiolin, 2011): a lower working temperature, the absence of droplets during the expansion, the low maintenance. The applications of Organic Rankine Cycle have the economic attractiveness when it is used at the small and medium power scales (Schuster, 2009).

In an ORC system, the turbine or expander plays a crucial role in the performance. Specification of the turbine technology depends on the operating conditions and the scale of the system. A radial inflow turbine is used in this study as it is suitable for small scale power generation (50kW-500kW) with low mass flow rate and high pressure ratio, as well as other motivations (Sauret, 2011): Radial inflow turbines require minor modifications for different geothermal resources; it is less sensitive to blade profile inaccuracies than axial turbines and more robust under increased blade load; it is easier to manufacture compared to axial machines; the rotor-dynamic stability of the radial inflow turbine is also improved due to a higher stiffness.

In this study, to conduct the design of the AGGAT turbine with 100kW power output, a single stage radial inflow turbine design was chosen, using R245fa as the working fluid due to its environmental characteristics, cost-effectiveness, thermal stability and properties (Bertrand, 2013; Liu, 2004; Lopez, 2013), to convert the geothermal energy into the mechanical energy in the ORC system.

When developing such an AGGAT radial inflow turbine, the aerodynamic design and the stress analysis are the vital steps in the turbine design system which consists of aerodynamic design, stress analysis, rotor dynamics analysis, manufacturing and testing. This paper presents the detailed information of the aerodynamic design (from 1D preliminary design to 3D modeling of turbine blades, passage and volute), and the stress analysis of turbine blades. Turbine performance is validated through CFD and the structural strength is evaluated by using FEM to confirm its safety.

2. AERODYNAMIC DESIGN

In the step of aerodynamic design, it consist of five components which are 1D preliminary design, blade profile and passage design, 3D geometry of blade and passage, 3D modeling of volute and 3D numerical simulation, as shown in Figure 2.

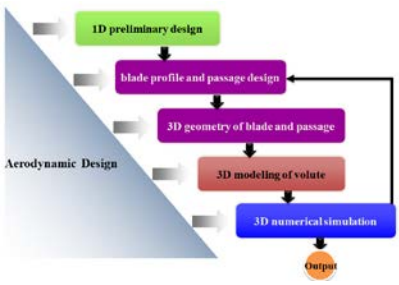

Figure 2: Aerodynamic design system of turbine

1D preliminary design is firstly conducted to get well-matched flow conditions, especially the flow angles at inlet and outlet of the stator and the rotor. The basic dimensions of the blades and passage are established in the preliminary design, which initiates the detailed design steps. Based on the results of 1D preliminary design, the blade profiles from the root section to the tip section are normally constructed by using camber line plus thickness method. After this, 3D geometry of the blade is generated by stacking the blade profiles from root section to tip section and 3D modeling of the volute is completed by employing the free vortex theory based on the radius and the flow conditions at the inlet. Finally, the 3D numerical simulation is performed to evaluate the turbine performance and make some modifications until the optimal results are achieved.

2.1 1D preliminary design

In this section, a set of stations are chosen at the inlet of every component of the turbine. Given the appropriate value of aerodynamic and thermodynamic parameters (mass flow rate, pressure ratio, fluid properties etc.), the thermodynamic and fluid dynamic conservation principles are applied at each station. After that, the results including the geometric dimension (blade heights, dimensions of inlet and outlet, axial length of blade etc.) and aerodynamic parameters (power, flow angles, Mach number, specific speed etc.) are output under the design point.

To conduct the preliminary design, three core correlations are used and they are optimum speed ratio, specific speed and specific diameter The optimum speed ratio plays a crucial role in the preliminary design of radial inflow turbine (Dixon, 2013; Barr, 2008; Shahhosseini, 2008; Wong, 2014), and it is defined as,

$$\frac{U}{C_0} = \frac{U}{\sqrt{2\Delta h_{is}}} \tag{1}$$

where U (m/s) is the tip speed of rotor and C_0 (m/s) is called spouting velocity. Spouting velocity is the velocity that has an associated kinetic energy equal to the isentropic enthalpy drop Δh_{is} from turbine inlet stagnation pressure to the final exhaust pressure. Generally, the optimum speed ratio is equal to about 0.7 for a good turbine under the design point (Marcuccilli, 2007). Apart from this, the application of specific speed N_s and specific diameter D_s was proposed for the radial inflow turbine design (Cordier, 1955; Balje, 1981; Wright, 2010; Ventura, 2012). N_s is mainly used to define the rotational speed of radial inflow turbine and D_s is to represent the characteristics diameter of turbine. The expressions are,

$$N_s = \frac{\omega\sqrt{m/\rho_{exit}}}{\Delta h_{is}} \tag{2}$$

$$D_s = \frac{D(\Delta h_{is})^{0.25}}{\sqrt{m/\rho_{exit}}} \tag{3}$$

where, ω is rotational speed of turbine rotor, m is mass flow rate across the turbine stage, ρ_{exit} is fluid density at the turbine outlet, Δh_{is} is isentropic enthalpy drop from the inlet to the outlet and it is the same as that of equation (1), and D is diameter of turbine rotor. According to the study of Balje (1981), the optimum ranges of specific speed and specific diameter are (0.4-0.9), (3-5) respectively.

Based on the correlations and expressions above, the 1D preliminary design is conducted by using the ANSYS Radial Turbine Design (RTD) module and the results are,

- Power: 115kW
- Optimum speed ratio: 0.698
- Specific speed: 0.6
- Isentropic efficiency: 0.87
- Rotor exit absolute flow angle: 0^o

2.2 3D modeling of turbine

This section presents the detailed design step for the AGGAT turbine based on the results from the 1D preliminary design. The design information of the stator and rotor blades and the volute is shown, and the performance evaluation and the analyses of the flow features across the turbine are performed.

2.2.1 Design method for turbine blades and passage

The design of the stator was conducted by using an in-house code which is developed based on the camber line plus thickness method, illustrated in Figure3. This method uses a third-order spline function for constructing the camber line and the thickness based on the flow angles calculated from the 1D preliminary design. After specifying the thickness

distribution, the stator is constructed based on the relations between the adjacent inscribed circles.

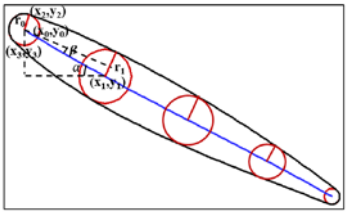

Figure 3: Design method of stator blade

In rotor design, ANSYS BladeGen module is used to carry out the modeling of turbine. Figure 4 shows the details of the BladeGen for rotor design. The passage is designed by using Fourth-order Bezier curve based on the passage dimension calculated in the 1D preliminary design step and the rotor is built through the camber line plus thickness method. The camber line angle Theta can be adjusted to change the expansion level of the fluid and the flow angle in order to ensure that the exit flow angle is nearly equal to zero.

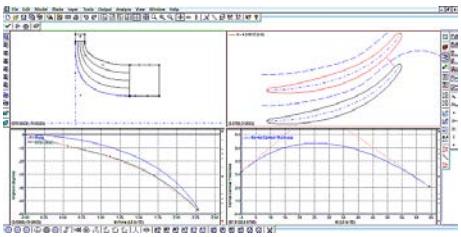

Figure 4: Rotor design using BladeGen

Moreover, this turbine is mounted on the same shaft with the generator. Therefore, the turbine thrust load should not exceed the limit of the magnetic bearings, which requires that the axial thrust load is less than 1600N. To further reduce the thrust load, a scalloped design (removes some parts between rotor blades at the inlet) of rotor and a balance piston on the shaft are performed in the study (Baskharone, 2006; Baines, 2003; Gupta, 2006; Faulkner, 2000; Childs, 1997; Hitachi, 1992).

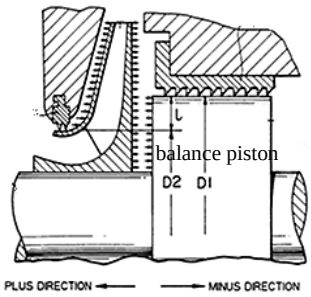

Figure 5：Balance piston in compressor (Hitachi, 1992)

Figure 5 shows the theory of reducing the thrust load in compressor and it is similar in turbine where the working fluid expands and generates the aerodynamic loading on the rotor blades and hub. Meanwhile, small proportion of the working fluid goes to the clearance between rotor and balance piston through the scallop, producing two forces which are in the opposite directions on rotor back face and balance. The diameter of balance piston can be optimized to reduce the net thrust load.

2.2.2 Design method for turbine volute

A volute is a unique component in turbomachinery that leads the fluid to go along the volute passage while entering into the stator passage. To reduce the flow loss and obtain uniform flow field in the volute passage, its sectional area should decrease gradually from the inlet to the tongue along the stream wise direction, as shown in Figure 5.

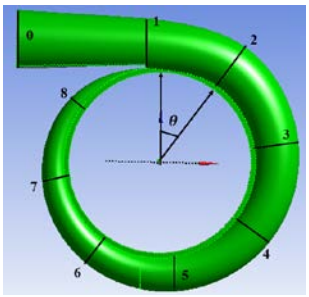

Figure 6: Volute sections

In this study, the circular section shape is adopted for the volute design and the volute is defined by a series of radial sections on the periphery of the turbine and the modeling of the circular sections is carried out by using the continuity and angular momentum theory.

The method for volute design is proposed by Xi (Xi, 2012) and the final expression of the circular section is,

$$c_u R_0 \rho_\theta 2\pi[R_0 + r - \sqrt{R_0(R_0+2r)}] = \frac{2c_r \rho \pi R_0 L(\theta_{\max} - \theta)}{\theta_{\max}} \quad (4)$$

where θ is the azimuth angle, $c_{\theta u}$ is the tangential component velocity, ρ_θ is the density at the section, $\theta_{\max}$ is the maximum azimuth angle.

2.3 Evaluation of turbine performance

The simulation was conducted to evaluate the turbine (including the stepped labyrinth seal) performance with R245fa as the working fluid and the detailed analysis on the flow field across the turbine passage and the leakage flow in the seal cavities was presented in this section.

Figure 7 shows the mesh with back plate gap and the stepped labyrinth seal for performance evaluation. Total mesh nodes are 16.5 million with the inflation layers near the wall.

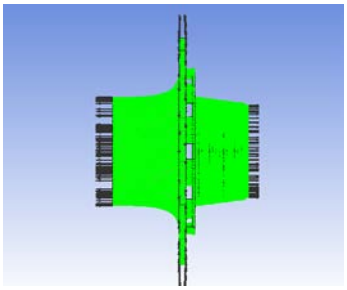

Figure 7 Mesh with back plate gap and stepped labyrinth seal for simulation

The simulation results including power, efficiency, rotational speed and net thrust load are shown in Table 1. The power output is 101.5kW with the isentropic efficiency of 0.85. The net thrust load is 131N by using the balance piston and it matches with the loading requirements of the magnetic bearings whilst maintaining the turbine performance nearly constant.

Table 1 Simulation results of turbine performance

Power (kW)	Isentropic efficiency	Rotational speed (rpm)	Net Thrust load (N)
101.5	0.85	29000	131

The total pressure distribution on the turbine stator and rotor is shown in Figure 8. The fluids enters the stator passage and the velocity increases when passing through with the total pressure decreasing from the inlet to the throat zone and it starts to expand further from the throat zone to the outlet. No separation flow is observed in the stator passage and it implies that the secondary flow loss is relatively low and the efficiency is high in stator. In addition, the total pressure of the fluid decreases more to generate mechanical power in the rotor passage.

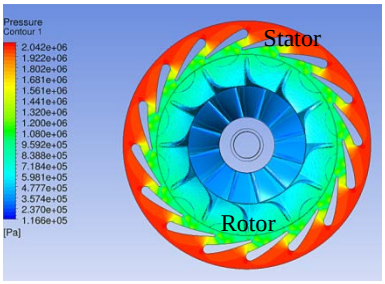

Figure 8 Total pressure distribution on turbine blades

The streamlines in the turbine passage including the back plate clearance and the seal are shown in Figure 9.

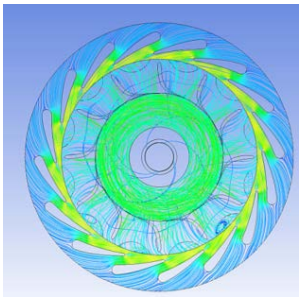

(a) Streamlines in turbine passage

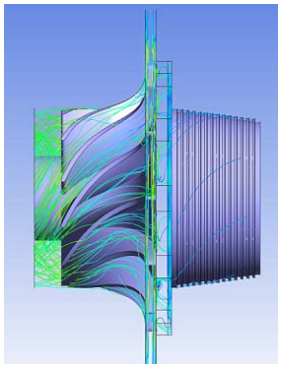

(b) Streamlines in turbine, back plate clearance and seal

Figure 9 Streamlines distribution in turbine, back plate clearance and seal

The streamlines go smoothly from the inlet to the outlet without separation flow in the stator passage. In the rotor passage, the tip leakage flow goes from the pressure side to the suction side and mixes with the main steam. According to Figure 9 (b)), the separation flows dominate the scallop path, the back plate clearance and the seal path. The separation flows in the scallop path and back plate clearance are not good to turbine performance and it causes high secondary flow loss and decreases the efficiency. The separation flow in the cavity of the seal path is beneficial for reducing the leakage flow from the turbine. The pressure of the leakage flow decreases gradually from the seal inlet to the outlet, through which, less fluid is leaking and more fluid is kept in the passage to produce power.

To understand the flow features in the back plate clearance, the total pressure and the wall shear contours are analyzed, as shown in Figure 10. It is obvious that there is high total pressure zone on the back plate face close to the rotor scallop, which is because the fluid goes through the rotor scallop path and crashes on the back plate face causing stagnation point there and then goes downward to the shaft in the clearance. The low pressure zone is resulted from the strong separation flow near the stagnation point at the back plate. While, the wall shear contour is similar to that of the total pressure. The high shear stress zone corresponds to the high total pressure zone and it implies the high entropy generation and low flow efficiency. The shear stress is relatively low at the zone near the balance piston where the fluid enters the labyrinth seal through the seal inlet.

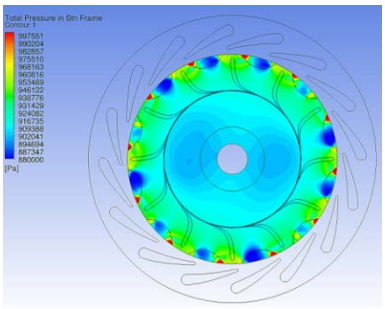

(a) Total pressure on back plate face and balance piston

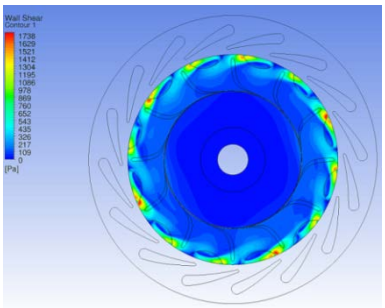

(b) Wall shear stress on back plate face and balance piston

Figure 10 Total pressure and wall shear stress on back plate face and balance piston

Figure 11 shows the static pressure distribution in the volute. We can see that the static pressure decreases smoothly from the inlet to the outlet without any obvious low pressure

zones. In addition, as the flow area decreases gradually from the inlet to the outlet, the velocity increases. In this way, the mass flow rate is kept constant. Thus, the pressure is relatively low at the outlet. Overall, the flow loss is very low and the efficiency is high in the volute passage.

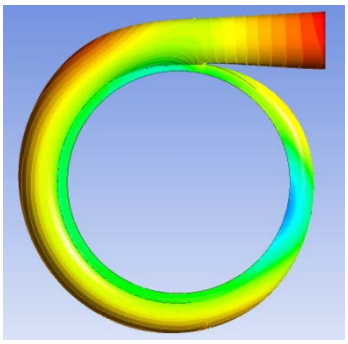

Figure 11 Pressure distribution in the volute

The streamlines distribution in the volute passage is presented in Figure 12. It shows a good flow condition in the volute passage from the inlet to the outlet without any separation flow, indicating the feasibility of the method for the volute design. The working fluid enters into the volute passage at the inlet and goes along the passage to the tongue with a uniform flow field.

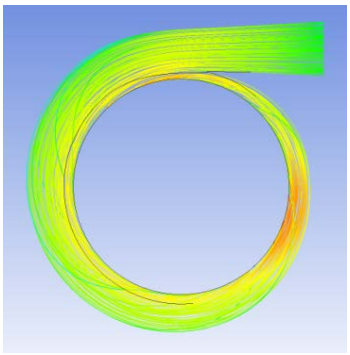

Figure 12 Streamlines in the volute

3. STRESS ANALYSIS OF TURBINE

This section presents the stress analysis of the turbine and the motivation of doing this is to ensure that the turbine has an adequate life in service after the turbine geometry has been defined. Failure of the turbine will happen if the maximum stress on the blades is greater than the yield strength of the material.

ANSYS Static Structural is used to conduct the stress analysis of stator and rotor blades and the material selection of each component is performed (Matweb material property), as shown in Table 2.

Table 2 Material selection of stator and rotor

Components	Stator and passage	Rotor
Materials	Alloy steel	Aluminum alloy
Yield tensile strength [MPa]	675	470
Poisson ratio	0.29	0.33
Shear Modulus [GPa]	80	25

3.1 Stress analysis of stator

The mesh of the stator and the shroud for stress analysis is shown in Figure 13. The total mesh nodes are 330653 with the fine mesh at the bolts areas.

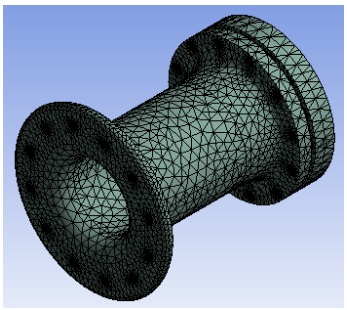

Figure 13 Mesh of stator for stress analysis

The force loading on the blades and passage calculated by the 3D simulation in Section 2.3 is specified for the stress analysis, as shown in Figure 14. The fixed support boundary was proposed for the bolts areas in the analysis.

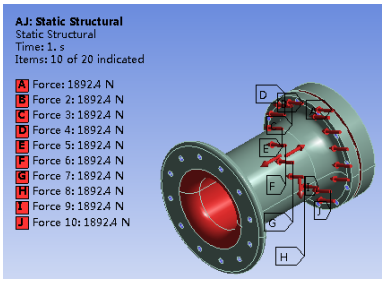

Figure 14 Setting of stress analysis of stator

Figure 15 shows the stress distribution on stator blades, hub and shroud. It can be noted that the equivalent stress on the stator hub and shroud is very low and the stress on the stator blades is higher than that on the hub and the shroud. The maximum stress is 57.4MPa which occurs at the trailing edge of stator blades. The safety factor of the stator is 675/57.4=11.8, which is much higher than the requirement of 1.5 for the industrial application.

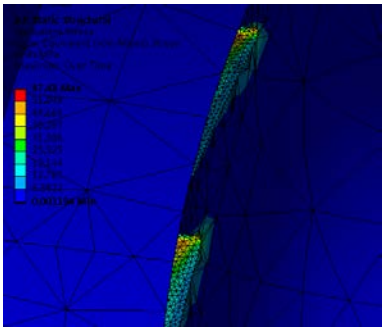

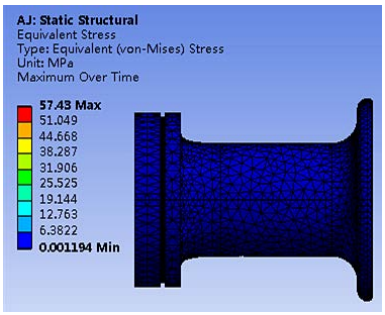

Figure 15 Equivalent Stress distribution of stator

The deformations of stator blades, hub and shroud are shown in Figure 16. The deformations of the shroud are higher than that of the hub due to higher loading on the shroud. The maximum deformation is located at the trailing edge of stator blades with the number of 0.0018mm, because the stress on the trailing edge is maximum and the thickness of the trailing edge is relatively small.

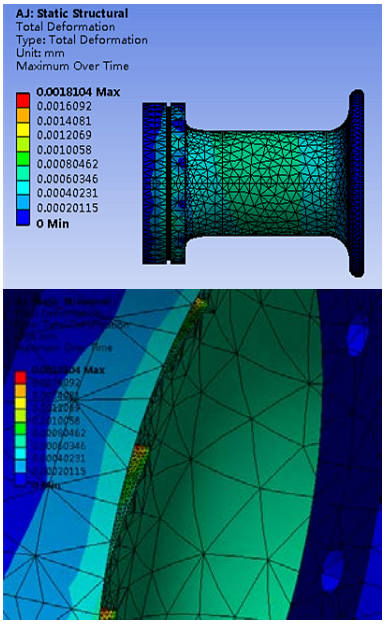

Figure 16 Deformation distribution of stator

3.2 Stress analysis of rotor

For the stress analysis of rotor, the mesh has similar nodes number to the stator and the force loading calculated by the CFD in Section 2.3 and the centrifugal forces due to its rotation are also concerned, as shown in Figure 17. The rotational speed of 29000 rpm is specified.

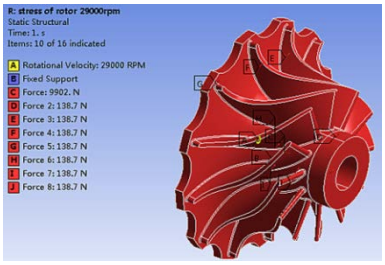

Figure 17 Setting of stress analysis of rotor

The stress distribution on the rotor hub and blades is shown in Figure 18. It can be seen that the peak stress on the rotor is 89.7MPa and it concentrates on the root of the rotor blades and the back of the hub close to the shaft, which results from the high rotational speed. The safety factor is 470/89.7=5.2 which is higher than 1.5 and it implies that the rotor has good stress distribution through the aerodynamic design (scallop design) and aluminum alloy is strong enough to handle the load on the rotor hub and blades, making it very safe during its operation. The low stress zone is noted at the leading edge, the tip section of the rotor near the trailing edge and the hub close to the exit.

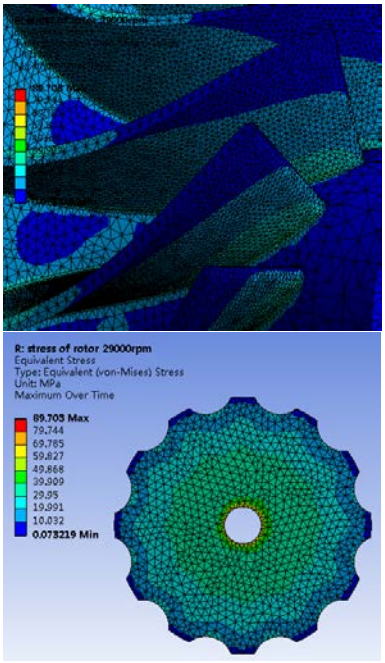

Figure 18 Equivalent Stress distribution of rotor

Figure 19 illustrates the deformation of the rotor hub and the blades due to the effect of the stress.

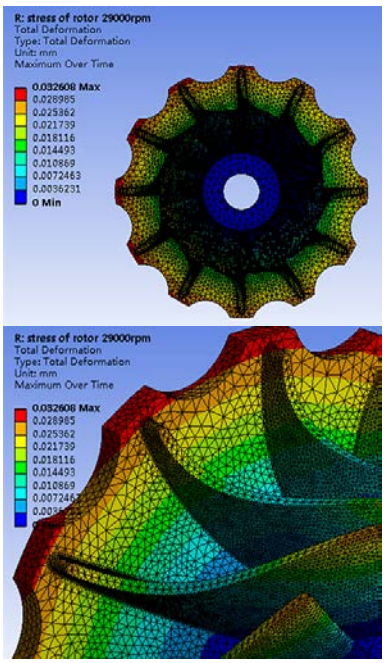

Figure 19 Deformation distribution of rotor

It can be observed that the maximum deformation of rotor is 0.032mm located at the tip section of the hub near the leading edge. The deformation at the tip section of the rotor trailing edge is higher than that in the middle of the blades and most of the hub zone. Although the stress at the leading edge and the trailing edge is low, the thickness of the leading edge and trailing edge is small which results in the high deformation of the rotor blades.

4. CONCLUSION

This paper presents the aerodynamic design and the stress analysis approaches for the development of the radial inflow turbine applied to Organic Rankine Cycle system using R245fa as the working fluid. The in-house code and the ANSYS turbomachinery module are used to conduct the turbine design based on the correlations of optimum speed ratio, specific speed and specific diameter. The 3D simulation results show that the turbine power is 101 kW with the isentropic efficiency of 0.85. The strong tip leakage flow of the rotor mixes with the main stream and the secondary flow dominates the scallop path, the back plate clearance and the seal path, casuing massive secondary flow loss and decreasing the flow efficiency. In addition, the stress analysis is conducted to evaluate its structural strength under the aerodynamic stress. Results show that the minumum safety factor is 5.2 which indicates that the turbine blades can handle the stress under the rotatinal speed of 29000 rpm.

This turbine design is in the manufacturing phase and HERA is working together with its partner to make the drawings more cost-effective in terms of manufacturing.

ACKNOWLEDGEMENTS

This work was part of the AGGAT programme funded by NZ Ministry for Business Innovation and Employment. The authors would like to thank the turbine research team in HERA for their helpful feedback. The authors would also like to thank Brent Young and Wei Yu for the access to ANSYS software and thank Rajnish Sharma for reviewing the design and the simulation work.

REFERENCES

Baines N C, Japikse D. Axial and radial turbines [M]. Wilder, VT: Concepts NREC, 2003.

Baines, N. ENGR408-ENME 627-SI Special topic in engineering: Turbomachinery. (2014).

Balje O E. Turbo-machinery: A Guide to design, Selection, and Theory [J]. (1981).

Barr L, Spence S W T, Eynon P. Improved performance of a radial turbine through the implementation of back swept blading[C]//ASME Turbo Expo 2008: Power for Land, Sea, and Air. American Society of Mechanical Engineers, 1459-1468. (2008).

Baskharone, Erian A. Principles of turbomachinery in air-breathing engines. Cambridge University Press, 2006.

Bertrand T F, Papadakis G, Lambrinos G, et al.: Criteria for working fluids selection in low-temperature solar organic Rankine cycles [C]//1st International Congress on Heating, Cooling and Buildings, Lisbon. (2013).

Boyce and Meherwan P. Gas turbine engineering handbook. Elsevier, 2011.

Childs, Dara W., and John M. Vance. "Annular gas seals and rotordynamics of compressors and turbines." Proceedings of the 26th Turbomachinery Symposium. 1997.

Cordier, O.. “Similarity considerations in turbomachines,” VDI Reports, 3. (1955).

Dixon S L, Hall C. Fluid mechanics and thermodynamics of turbomachinery[M]. Butterworth-Heinemann. (2013).

Faulkner, Lynn, and Earl Logan Jr, eds. Handbook of machinery dynamics. CRC Press, 2000.

Gupta, Manoj K., and Dara W. Childs. "Rotordynamic Stability Predictions for Centrifugal Compressors Using a Bulk-Flow Model to Predict Impeller Shroud Force and Moment Coefficients." ASME Turbo Expo 2006: Power for Land, Sea, and Air. American Society of Mechanical Engineers, 2006.

Hitachi, http://www.google.com/patents/EP0550801B1?cl=en

Liu B T, Chien K H, Wang C C. Effect of working fluids on organic Rankine cycle for waste heat recovery [J]. Energy,29(8): 1207-1217. (2004).

Lopez Sanz E. Study on a radial turbine stage with inlet guide vanes for an orc process with an electrical output of 3, 5 kW [J]. (2013).

Marcuccilli F, Zouaghi S. Radial inflow turbines for Kalina and organic Rankine cycles [J]. system, 2: 1.(2007).

Matweb material property data, http://www.matweb.com

Quoilin S, Orosz M, Hemond H: Performance and design optimization of a low-cost solar organic Rankine cycle for remote power generation [J]. Solar Energy, 85(5): 955-966. (2011).

Quoilin S, Van Den Broek M, Declaye S: Techno-economic survey of Organic Rankine Cycle (ORC) systems [J]. Renewable and Sustainable Energy Reviews, 22: 168-186. (2013).

Sauret E, Rowlands A S.: Candidate radial-inflow turbines and high-density working fluids for geothermal power systems [J]. Energy, 36(7): 4460-4467. (2011).

Schuster A, Karellas S, Kakaras E: Energetic and economic investigation of Organic Rankine Cycle applications [J]. Applied thermal engineering, 29(8): 1809-1817. (2009).

Shahhosseini M R, Hajilouy-Benisi A, Rad M. Numerical and Experimental Investigation of the Flow and Performance Characteristics of Twin-Entry Radial Turbine Under Full and Partial Admission Conditions[C]//ASME Turbo Expo 2008: Power for Land, Sea, and Air. American Society of Mechanical Engineers, 1507-1517. (2008).

Ventura C A M, Jacobs P A, Rowlands A S, et al. Preliminary design and performance estimation of radial inflow turbines: An automated approach [J]. Journal of Fluids Engineering, 134(3): 031102. (2012).

Wong C S, Krumdieck S. Energy and exergy analysis of an air-cooled geothermal power plant with fixed nozzle turbine subsonic expansion and supersonic expansion via CFD analysis[C]//Proceedings 36th New Zealand Geothermal Workshop, 24: 26. (2014).

Wright T., Gerhart Philip. Fluid machinery: application, selection, and design [M]. CRC press. (2010).

Xi Zhong. Investigation on aerodynamic design and optimization method for radial turbine [D]. Graduate University of Chinese Academy of Sciences (Institute of Engineering Thermophysics). (2012).